11220 *Biochemistry* **2009,** *48,* 11220–11230
DOI: 10.1021/bi901606n

BIOCHEMISTRY
including biophysical chemistry & molecular biology
Article

NMR Spectroscopic Characterization of the Sialyltransferase CstII from *Campylobacter jejuni*: Histidine 188 Is the General Base[†]

Patrick H. W. Chan,[‡,§] Luke L. Lairson,[∥] Ho Jun Lee,[‡,§] Warren W. Wakarchuk,[⊥] Natalie C. J. Strynadka,[‡,§,#,△] Stephen G. Withers,[‡,§,∥] and Lawrence P. McIntosh*[,‡,§,∥,△]

[‡]*Department of Biochemistry and Molecular Biology, University of British Columbia, Vancouver, BC, V6T 1Z3 Canada,* [§]*Centre for High-throughput Biology, University of British Columbia, Vancouver, BC, V6T 1Z4 Canada,* [∥]*Department of Chemistry, University of British Columbia, Vancouver, BC, V6T 1Z1 Canada,* [⊥]*Institute for Biological Sciences, National Research Council Canada, Ottawa, ON, K1A 0R6 Canada,* [#]*Centre for Blood Research, University of British Columbia, Vancouver, BC, V6T 1Z3 Canada, and* [△]*Michael Smith Laboratories, University of British Columbia, Vancouver, BC, V6T 1Z4 Canada*

Received September 15, 2009; Revised Manuscript Received October 11, 2009

ABSTRACT: Cell surface glycans are often terminated by sialic acid, which is incorporated onto sugar acceptors by sialyltransferases. The crystal structure of the GT family 42 *Campylobacter jejuni* α-2,3/2,8-sialyltransferase (CstII) provides key insights into the sialyl-transfer mechanism, including tentative identification of His188 as the catalytic base. In support of this hypothesis, the CstII-H188A mutant is able to catalyze sialyl transfer from CMP-Neu5Ac to added anions such as azide and formate but not to its natural sugar acceptor lactose. Complementing this work, NMR spectroscopy was used to investigate the structure and dynamics of CstII and to measure the intrinsic pK_a value of His188 for comparison with the pK_a determined from the pH-dependent k_{cat}/K_M of the enzyme. By systematically introducing point mutations at the subunit interfaces, two active monomeric variants, CstII-F121D and CstII-Y125Q, were obtained and characterized. In contrast to the wild-type tetramer, the monomeric CstII variants yielded good quality $^1H/^{15}N$-HSQC and $^1H/^{13}C$-methyl-TROSY NMR spectra. However, the absence of signals from approximately one-half of the amides in the $^1H/^{15}N$-HSQC spectra of both monomeric forms suggests that the enzyme undergoes substantial conformational exchange on a millisecond to microsecond time scale. The histidine pK_a values of CstII-F121D in its apo form were measured by monitoring the pH-dependent chemical shifts of [$^{13}C^{\varepsilon 1}$]histidine, biosynthetically incorporated into the otherwise uniformly deuterated protein. Consistent with its proposed catalytic role, the site-specific pK_a value ~6.6 of His188 matches the apparent pK_a value ~6.5 governing the pH dependence of k_{cat}/K_M for CstII toward CMP-Neu5Ac in the presence of saturating acceptor substrate.

Glycosyltransferases (GT's)[1] are enzymes that incorporate residues from a nucleotide sugar donor onto a sugar acceptor. They are classified by the carbohydrate active enzymes database (CAZy) into at least 91 families based on amino acid sequence, structure, and catalytic mechanism (*1*). Sialyltransferases (ST's) in the Golgi transfer the essential 9-carbon sugar sialic acid, or *N*-acetylneuraminic acid (Neu5Ac), onto various acceptors such as lactose that are then displayed on the cell surface in the form of glycolipids and glycoproteins. Sialic acids are involved in many important physiological functions, including cell growth and differentiation, cell−cell interactions (*2*), and bacterial and viral pathogenesis (*3*). Examples include sialic acids within lipooligosaccharides (LOS's) on the bacterial cell surface (*4*) and in the gangliosides of human nerve cells (*5*). *Campylobacter jejuni* is a common human food-borne pathogen that causes diarrhea and can give rise to neurodegenerative autoimmune diseases such as Guillain−Barré and Miller−Fisher syndromes (*6*). The autoimmune reaction is directed to gangliosides in nerve tissue as *C. jejuni* displays sialylated LOS's that mimic the gangliosides on human cells (*7*). Thus, ST's are also virulence factors, closely linked to the potential of microorganisms to cause serious disease.

Among the ST's identified in *C. jejuni*, crystal structures of the bifunctional α-2,3/2,8-sialyltransferase (CstII) and the monofunctional α-2,3-sialyltransferase (CstI) have been solved (*8*, *9*). Both CstI and CstII belong to GT family 42 and use an inverting mechanism for sialyl transfer, forming an α-2,3 linkage to acceptor sugars containing a terminal galactose residue (Figure 1).

[†]This research was supported by grants from the Natural Sciences and Engineering Research Council of Canada (L.P.M., S.G.W.) and the Canadian Institutes for Health Research (W.W.W., N.C.J.S., S.G.W.). S.G.W. is the recipient of a Canada Research Chair in Chemical Biology. Instrument support was provided by the Canadian Institutes for Health Research, the Canada Foundation for Innovation, the British Columbia Knowledge Development Fund, the UBC Blusson Fund, and the Michael Smith Foundation for Health Research.

*To whom correspondence should be addressed at the Department of Biochemistry and Molecular Biology, Life Sciences Centre, University of British Columbia. E-mail: mcintosh@chem.ubc.ca. Phone: 604-822-3341. Fax: 604-822-5227.

[1]Abbreviations: CD, circular dichroism; CMP-Neu5Ac, cytidine-5′-monophospho-*N*-acetylneuraminic acid; CMP-3FNeu5Ac, CMP-3-fluoro-*N*-acetylneuranminic acid; CstI, *Campylobacter* α-2,3-sialyltransferase; CstII, *Campylobacter* α-2,3/2,8-sialyltransferase; ESI-MS, electrospray ionization mass spectrometry; GT, glycosyltransferase; HEPES, 4-(2-hydroxyethyl)-1-piperazineethanesulfonic acid; HSQC, heteronuclear single-quantum correlation; IPTG, isopropyl β-D-1-thiogalactopyranoside; KIE, kinetic isotope effect; LOS, lipooligosaccharide; MES, 2-(*N*-morpholino)ethanesulfonic acid; Neu5Ac, *N*-acetylneuraminic acid; NMR, nuclear magnetic resonance; PBS, phosphate-buffered saline; pH*, the pH meter reading without correction for isotope effects; pK_a*, the apparent pK_a value without correction for isotope effects; ST, sialyltransferase; TLC, thin-layer chromatography; T_m, midpoint unfolding temperature; TROSY, transverse relaxation optimized spectroscopy.

 Published on Web 10/13/2009

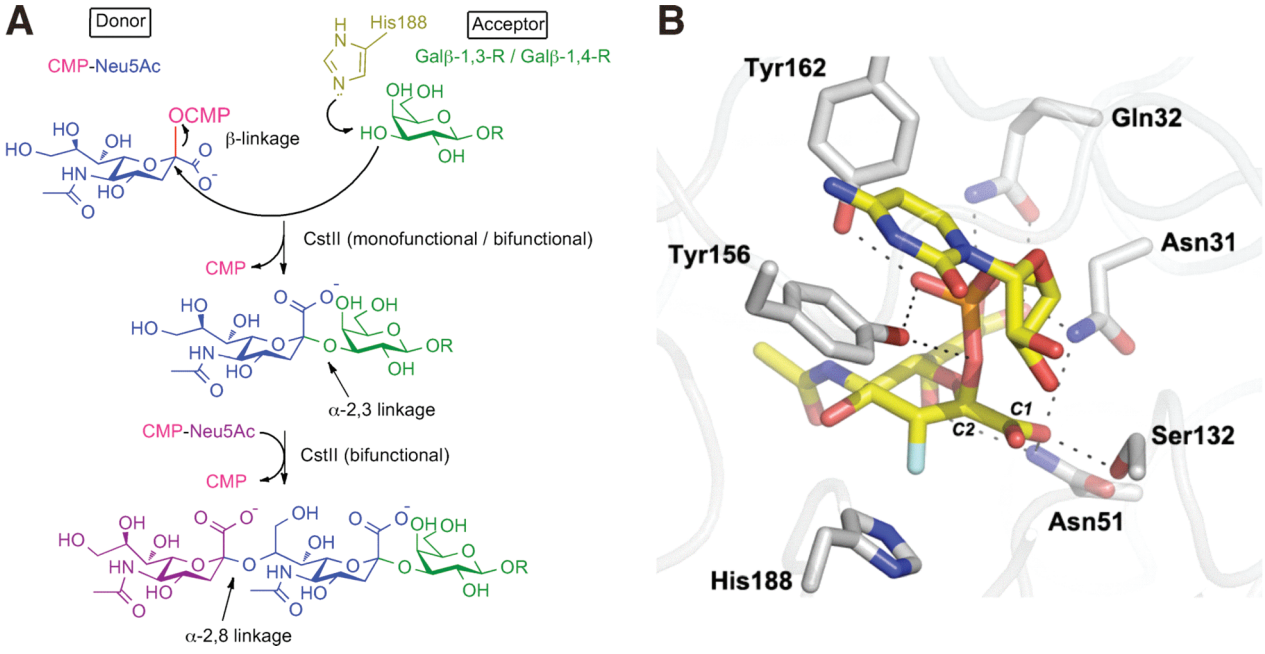

FIGURE 1: (A) Inverting sialyltransferase reaction catalyzed by CstII. Monofunctional and bifunctional CstII both catalyze formation of an α-2,3 linkage between donor CMP-Neu5Ac and an acceptor. The bifunctional CstII can subsequently add an α-2,8-linked-Neu5Ac to the initial product. (B) Wild-type CstII active site highlighting the side chain imidazole of His188 suitably positioned on the α-face of the donor substrate analogue CMP-3FNeu5Ac to play the role of base catalyst. Atoms are colored according to type (C, gray or yellow; N, blue; O, red; F, cyan; P, orange) and the carboxyl (C1) and anomeric (C2) carbons of CMP-3FNeu5Ac labeled.

Although the sequences of CstI and CstII are only 42% identical, they use common amino acid residues for substrate binding and catalysis, and their overall structures in complex with a deactivated donor substrate analogue, CMP-3FNeu5Ac, are similar (*8*, *9*). Furthermore, there are monofunctional (OH19) and bifunctional (OH4384) variants of CstII. In addition to α-2,3-sialyl transfer, bifunctional CstII also has α-2,8-sialyltransferase activity, adding an additional Neu5Ac to the initially incorporated α-2,3-linked sialoside. The sequences of the two CstII variants are 97.3% identical (*10*), and thus the difference of only eight amino acid residues determines the additional activity in the latter enzyme (*11*). Both CstI and CstII are tetrameric, and each monomer subunit contains two domains (*8*, *9*). One consists of a mixed α/β Rossmann fold nucleotide-binding domain. The second domain, composed of a long coil and two helices, forms a flexible "lid" over the active site. This lid domain is only ordered in the crystal structure of CstII complexed with CMP-3FNeu5Ac (*8*).

Prominent among the active site residues of CstI and CstII is a histidine (His202 and His188, respectively) proposed to serve as the general base that abstracts the proton from the nucleophilic hydroxyl group of the sugar acceptor, thereby facilitating attack on CMP-Neu5Ac (Figure 1). This is a somewhat unusual residue to serve as the base for glycosyl-transfer reactions. In essentially all glycoside hydrolases and in the majority of inverting nucleotide phospho-sugar glycosyltransferases, this role is performed by glutamate or aspartate residues (whereas retaining glycosyltransferases appear to use the departing phosphate moiety (*12*)). Histidine residues have only been proposed as general bases in GT 42 sialyltransferases, along with a subgroup of the GT-B fold family GT 1 inverting enzymes (*12*). Although mutational studies have confirmed their overall importance for catalysis, no definitive evidence for these histidine residues serving as a base has been provided. Thus, two avenues have been followed in this current study to test this proposal. First, "chemical rescue" experiments verified that an otherwise inactive H188A mutant of CstII can still catalyze the side reaction of CMP-Neu5Ac with anions including azide and formate. Second, NMR spectroscopy was used to measure the site-specific pK_a value of His188 for comparison with that determined by kinetic analysis. Preliminary NMR studies were foiled by the high molecular mass (~128 kDa) of the tetrameric enzyme (C. Chiu, Ph.D. Thesis, University of British Columbia, 2007). Fortunately, the active sites of CstI and CstII are contained entirely within a monomer subunit. By introducing point mutations at the subunit interfaces, two active monomeric variants of CstII were obtained, thereby enabling these NMR measurements. In support of its proposed role as a catalytic general base, the pK_a value of ~6.6 determined by NMR-monitored titrations of monomeric CstII indeed closely matches that of pK_a value ~6.5 governing its pH-dependent activity (k_{cat}/K_M).

MATERIALS AND METHODS

Site-Directed Mutagenesis. The previously described gene encoding "wild-type" CstII, with the mutation I53S and a deletion of the C-terminal 32-residue membrane association sequence, was cloned into the pET28a vector for expression as a His_6-tagged construct (*8*). Additional mutations were introduced sequentially using the QuikChange site-directed mutagenesis kit (Stratagene).

Protein Expression and Purification. The His_6-tagged proteins were expressed in *Escherichia coli* BL21(λDE3) cells according to previously published methods (*8*, *9*). The cells were grown at 37 °C to an OD_{600} of 0.8 and then induced with 1 mM IPTG. After further growth at 30 °C for 16 h, the cells were harvested by centrifugation and lysed by sonication in the presence of 50 mg/L lysozyme (Sigma). The cell debris was removed by centrifuging at 15000 rpm, and CstII was isolated from the supernatant using a HisTrap HP column (GE Healthcare). After thrombin digestion, HisTrap HP and HiTrap benzamidine FF columns (GE Healthcare) were used to remove

the His_6tag, uncleaved His_6-tagged proteins, and the protease. The N-terminal tripeptide Gly-Ser-His, or in the case of samples for histidine titrations, Gly-Ser-Gly, remained after cleavage of the tag. ^{15}N-labeled proteins were expressed in M9 minimal media containing 1 g/L $^{15}NH_4Cl$. Proteins selectively labeled with Ile$^{\delta1}$-[$^1H/^{13}C$], Leu-[$^{13}CH_3$,$^{12}CD_3$], and Val-[$^{13}CH_3$,$^{12}CD_3$] in an otherwise deuterated background were expressed in M9 media containing 70 mg/L 4-[^{13}C,^1H]-3,3-^2H-α-ketobutyrate, 120 mg/L 2-keto-3-methyl-d_3-3-d_1-4-^{13}C-butyrate (α-ketoisovalerate deuterated at the β-position and with one of the two methyl groups $^{13}CH_3$ and the other $^{12}CD_3$), 1 g/L $^{15}NH_4Cl$, and 3 g/L D-[^2H]-glucose in 99% D_2O (Cambridge Isotope Laboratories) (*13*−*15*). Proteins selectively labeled with [$^{13}C^{\varepsilon1}$]histidine in an otherwise deuterated background were expressed in the histidine auxotrophic strain BL21(λDE3) *hisG*, grown in M9 media containing 50 mg/L [$^{13}C^{\varepsilon1}$]-L-histidine (Icon Isotopes), 1 g/L NH_4Cl, and 10 g/L D-glucose in 99% D_2O (*16*, *17*). Unless stated otherwise, the purified proteins were exchanged into 20 mM Tris, 150 mM NaCl, and 5 mM DTT, pH 7.5, in H_2O or D_2O, using an Amicon Ultra-15 centrifugal filter device. Protein concentrations were determined by UV absorbance using predicted ε_{280} values of 34270 M^{-1} cm^{-1} for CstII-Y125Q and 35760 M^{-1} cm^{-1} for both wild-type CstII and CstII-F121D (*18*).

Activity Assays. The activities of unpurified mutants in cell lysates (induced with 1 mM IPTG and expressed overnight at 30 °C) were determined qualitatively by a TLC fluorescent assay using CMP-Neu5Ac and bodipy-lactose (*19*). Steady-state kinetic parameters for purified CstII and CstII-Y125Q were determined by a continuous coupled enzyme assay (*20*).

pH Dependence of k_{cat}/K_M. The pH dependence of k_{cat}/K_M for CstII was determined using the method of substrate depletion at low concentration ([S] ≪ K_M) of donor substrate (50 μM CMP-Neu5Ac) and saturating concentration of the acceptor substrate (15 mM 3′-sialyllactose). Rates of reaction were measured using a continuous coupled assay (*20*). Reactions were performed using 100 mM buffer with coupling components at 37 °C and initiated by the addition of 23 μg/mL purified enzyme (*20*). Assays were carried out at pH values ranging from 5.5 to 9.0 using 20 mM buffers as follows: sodium citrate for pH 5.5−6.0, MES for pH 6−6.5, sodium phosphate for pH 6.0−7.5, HEPES for pH 7.0−8.0, and Tris for pH 7.5−9.0. Overlapping data points indicated no significant dependence of activity on the specific buffer identity. A linear relationship between observed rates and CstII concentrations was observed at all pH values. Release of CMP, coupled to the oxidation of NADH (λ = 340 nm, ε = 6.22 mM^{-1} cm^{-1}), was monitored continuously at 340 nm for a minimum of 10 min, and the data were fit to the first-order rate equation using Grafit 5.0 (Erithacus Software). The resulting rate constant, adjusted for enzyme concentration, gives the k_{cat}/K_M for a given pH value. Data for k_{cat}/K_M dependence on pH were fit to a single ionization equilibrium curve using Grafit 5.0 to determine an apparent pK_a.

Anion Rescue Studies. Chemical rescue of the CstII-H188A mutant was performed using the continuous coupled assay (*20*). Initial rates for the CstII-H188A (16 μM) and wild-type enzyme (0.8 μM in monomer subunits) were determined at 0.5 mM CMP-Neu5Ac with varying concentrations of sodium formate (0−1 M) or sodium azide (0−0.25 M). Formation of an α-linked sialyl azide derivative was confirmed by negative ion mode ESI-MS and by the observed ability of *Clostridium perfringens* sialidase to convert the putative species to sialic acid, as determined by TLC analysis (4:2:1:0.1 EtOAc:MeOH:H_2O:AcOH).

Table 1: Data Collection and Refinement of CstII-Y125Q in Complex with CMP-3FNeu5Ac

Data Collection	
space group	*I*4
a (Å)	116.63
b (Å)	116.63
c (Å)	45.39
α, *β*, *γ* (deg)	90, 90, 90
wavelength (Å)	1.5418
resolution (Å)[a]	34−2.25 (2.37−2.25)
R_{sym} (%)[b]	5.9 (30.7)
$I/\sigma(I)$	18.4 (3.8)
completeness (%)	100 (100)
unique reflections	14714 (2137)
redundancy	4.1 (4.0)
Refinement Statistics	
average *B*-factors (Å^2)	
protein	20.6
substrate	48.4
water	25.3
Ramachandran statistics	
favored regions (%)	95.8
allowed regions (%)	4.2
R_{work} (%)[c]	17.7
R_{free} (%)[c]	21.9
rms[d] bonds (Å)	0.013
rms angles (deg)	1.366

[a]Values in parentheses represent the highest resolution shell. [b]$R_{sym} = \sum|I_{(hkl)} - \langle I\rangle|/\sum I_{(hkl)}$, where $I_{(hkl)}$ is the measured intensity of a given reflection and $\langle I\rangle$ is the average intensity of all symmetry equivalent measurements. [c]$R_{work} = \sum||F_o| - |F_c||/\sum|F_o|$, where F_o and F_c are observed and calculated structure factors, respectively. 5% of total reflections were excluded from the refinement to calculate R_{free}. [d]rms, root mean square.

Analytical Size Exclusion Chromatography and Static Light Scattering. The oligomerization states of CstII mutants were determined using a Sephacryl S-200 high-resolution XK16/60 gel filtration column (GE Healthcare), equilibrated with buffer (5 mM PBS, pH 7.4) connected to the mini-DAWN light scattering equipment coupled to an interferometric refractometer (Wyatt Technology) at 22 °C. Data analysis was performed in real time using ASTRA software (Wyatt Technology).

CD Spectroscopy. CD spectra of ∼10 μM protein in a 0.2 cm path length cuvette were recorded on a Jasco J810 spectropolarimeter. Four scans at 50 nm/min were averaged, followed by subtraction of a buffer blank spectrum. Thermal denaturation measurements were monitored at 220 nm with heating at a rate of 1 °C/min. Midpoint unfolding temperatures (T_m) were determined by fitting to a standard two-state model (*21*).

X-ray Crystallographic Analysis of CstII-Y125Q. Crystals of the CstII-Y125Q mutant (6.4 mg/mL) were grown by the hanging-drop vapor diffusion technique at 21 °C with 10 mM CMP-3FNeu5Ac in a mother liquor containing 75 mM tribasic ammonium citrate, pH 8.0, and 14% (w/v) PEG-3350. X-ray diffraction data were collected with 15% ethylene glycol as a cryoprotectant at 100 K under a nitrogen stream using an in-house Cu Kα rotating anode X-ray generator coupled to a Mar345 detector. The crystal belongs to the space group *I*4 with unit cell dimensions *a* = 116.63 Å, *b* = 116.63 Å, and *c* = 45.39 Å and contains one molecule in the asymmetric unit. Collected data were processed by MOSFLM (*22*) and the CCP4 suite of programs (*23*). All statistics for data collection and refinement are summarized in Table 1.

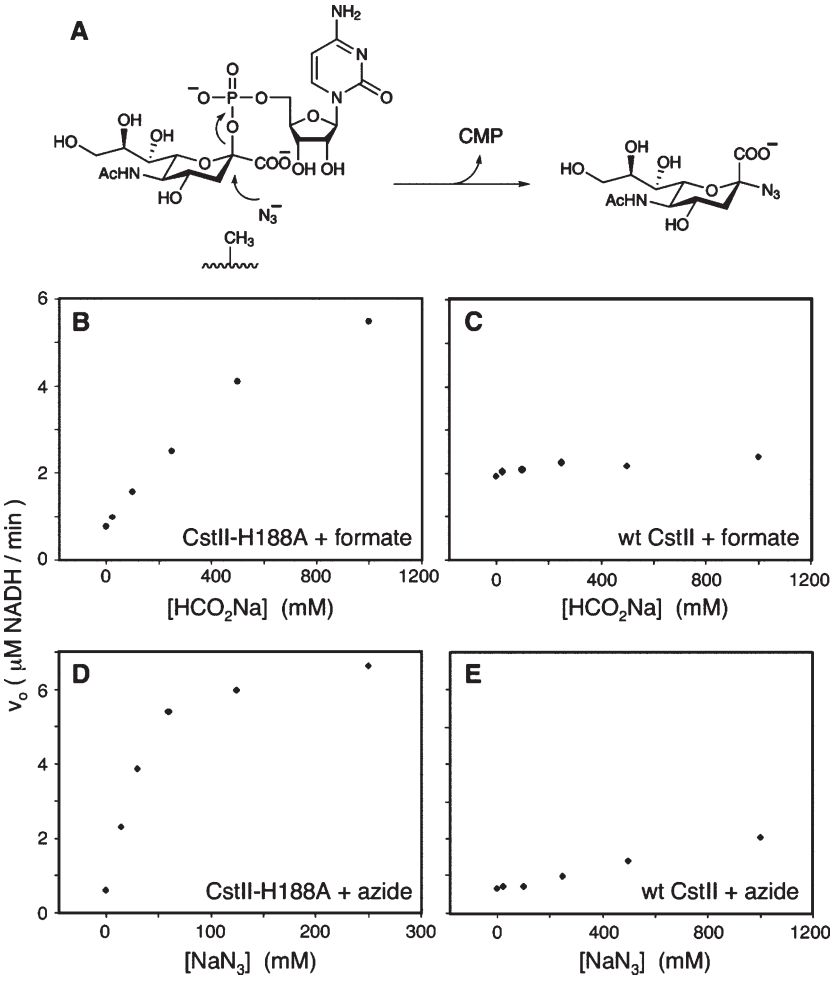

FIGURE 2: Chemical rescue of CstII-H188A by exogenous anions. (A) Schematic diagram of the chemical rescue experiment. Rates were determined using 16 μM (monomer subunits) CstII-H188A mutant or 0.8 μM wild-type enzyme, 500 μM CMP-Neu5Ac, 160 mM lactose, and standard CstII assay conditions. Increasing concentrations of formate and azide rescue the activity of CstII-H188A (B, D) without substantially influencing wild-type CstII (C, E).

The structure of CstII-Y125Q was solved by molecular replacement with PHASER (*24*) using the monomer of wild-type CstII (PDB accession code 1RO7) as the starting model. Subsequent model building was performed manually by COOT (*25*), and refinements were carried out by REFMAC (*26*), excluding 5% of reflections for the *R*-free calculation. The quality of the final model was validated using MolProbity (*27*). The CMP-3FNeu5Ac ligand model and its refinement restraints were generated from the PRODRG server (*28*). All structural figures were generated using PyMOL (*29*). The coordinates of CstII-Y125Q have been deposited in the Protein Data Bank under the accession code 2WQQ.

NMR Spectroscopy. NMR spectra were acquired at 25 °C on a Varian Inova 600 MHz spectrometer equipped with a cryogenic $^{1}H/^{2}H/^{13}C/^{15}N$ probe. Spectra were processed using NMRPipe (*30*) and analyzed with SPARKY 3 (*31*). One-bond sensitivity-enhanced $^{1}H/^{15}N$-HSQC spectra (*32*) were recorded for ^{15}N-labeled CstII, CstII-F121D, and CstII-Y125Q. $^{1}H/^{13}C$-methyl-TROSY and relaxation dispersion methyl-TROSY experiments (*13*, *14*, *33*, *34*) were recorded with [$^{1}H/^{13}C$]methyl-labeled deuterated CstII-Y125Q (0.1 mM) in D_2O sample buffer with or without 5 mM CMP-3FNeu5Ac. One-bond sensitivity-enhanced $^{1}H/^{13}C$-HSQC spectra with a CPMG pulse train (*35*) was recorded as a function of pH* with [$^{13}C^{\varepsilon 1}$]histidine-labeled CstII-F121D and CstII-F121D-H188A in D_2O sample buffer. The sample pH* values were adjusted by addition of microliter amounts of 0.05 M DCl and 0.05 M NaOD and measured using a NMR tube microprobe electrode (IQ Scientific Instruments). pK_a* values were determined by simultaneously fitting the resulting pH-dependent $^{1}H^{\varepsilon 1}$ and $^{13}C^{\varepsilon 1}$ chemical shifts to standard equations for the ionization of a single group using Matlab (MathWorks). The standard deviations of fit pK_a values were determined with a Monte Carlo approach using estimated errors of 0.05 in pH*, 0.04 ppm in ^{1}H, and 0.2 ppm in ^{13}C. The observed pH meter readings, denoted as pH*, were not corrected as the apparent pK_a* values determined in D_2O are approximately the same as those determined in H_2O due to compensating isotope effects on the acid dissociation equilibrium and the glass electrode (*36*).

RESULTS

Chemical Rescue of CstII-H188A Activity. Chemical rescue is a powerful approach for confirming the locations and identities of residues involved in acid/base or nucleophilic catalysis by glycoside hydrolases. It involves the demonstration of rescue of steady-state activity by mutants modified at the position in question upon the addition of exogenous anions such as azide (*37*−*39*) (Figure 2A). This approach has also been applied to probe nucleophiles in retaining GT's (*40*) but not previously to acid/base residues in this class of enzymes.

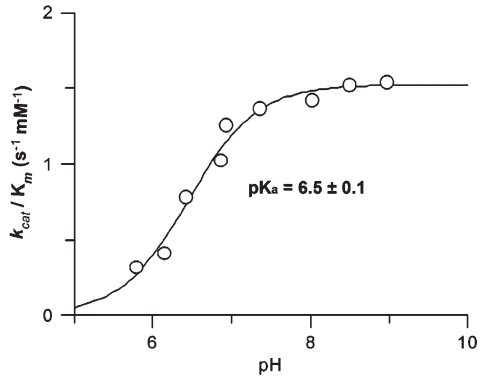

FIGURE 3: pH dependence of k_{cat}/K_M for utilization of CMP-Neu5Ac by CstII, saturated with sialyllactose, at 37 °C. The apparent pK_a value (and standard error) of 6.5 ± 0.1 was determined by best fit of the data to a single ionization equilibrium.

Mutation of His188 to alanine severely impairs CstII activity (*8*). Addition of either formate or azide to the CstII-H188A mutant resulted in significant concentration-dependent increases in its ability to utilize CMP-Neu5Ac as a substrate (Figure 2B,D). In contrast, wild-type CstII is relatively insensitive to these exogenous anions (Figure 2C,E). This behavior is completely consistent with anion rescue occurring exclusively with the mutant. Importantly, rates in the presence of lactose were virtually identical to those in the absence of this acceptor at all concentrations of exogenous nucleophiles. This indicates that the observed chemical rescue is not due to transferase activity involving lactose but rather arises through a diversionary pathway in which a sialic acid derivative is formed. Confirmation of this pathway was obtained by TLC and ESI-MS analyses of reaction mixtures, demonstrating the formation of a sialyl azide derivative by the H188A reaction mixture. Thus, removal of the side chain of His188 allows rescue by azide, thereby indicating that His188 is located close to the anomeric carbon of CMP-Neu5Ac and the 3′-OH group of lactose in the CstII active site. The distance and proximity are consistent with the proposed catalytic role of His188 (Figure 1).

pH-Dependent Activity of CstII. In order to assess the pK_a values of catalytic residues involved in essential proton transfer steps, the k_{cat}/K_M value for CstII-catalyzed reaction of CMP-Neu5Ac in the presence of saturating concentrations of sialyllactose was measured as a function of pH. As shown in Figure 3, the activity of CstII increases with pH, reaching a maximal plateau value near pH 8. The data fit a single ionization event with an apparent pK_a value of 6.5 ± 0.1. This kinetic pK_a likely reflects the deprotonation of the postulated general base, His188. To test this hypothesis, we used NMR spectroscopy to independently measure the pK_a value of His188 in a monomerized CstII variant.

Monomerization of CstII. The active site of tetrameric wild-type CstII is contained entirely within a monomer unit, and thus it was hypothesized that mutations at the subunit interface would not dramatically affect the activity of the enzyme. Based on intermonomer contacts and accessible surface areas, determined with the PROTORP server (*41*), key interfacial residues were identified as Tyr60′, Lys63′, Asp97′, Tyr98′, Pro100′, Asp101′, and Lys253′ on one subunit and Ala84, His85, Lys113, Ala117, Phe121, Ile124, Tyr125, and Phe126 on the other (Figure 4B). As summarized in Table 2, several of these were mutated individually or in various combinations to charged or polar residues. Fortunately, many of the resulting proteins were active based on a qualitative TLC assay. The remainder, particularly those with multiple mutations, either expressed poorly in *E. coli* or were inactive.

The oligomerization states of the active mutants were determined by analytical gel filtration chromatography. CstII-K63D and CstII-D97A remained tetrameric, whereas CstII-K253Q appeared as a mixture of dimeric and monomeric forms. Importantly, CstII-F121D and CstII-Y125Q had longer retention times, thus were identified as monomers. Confirming this conclusion, CstII-Y125Q was found by static light scattering to have a molecular mass of ~36 kDa, whereas that of wild-type CstII was ~140 kDa (Supporting Information Figure S1).

The kinetic properties of wild-type CstII and CstII-Y125Q were compared using a coupled assay (*20*) (Table 3). The k_{cat} and K_M values for CMP-Neu5Ac in the presence of saturating lactose were lower for CstII-Y125Q than for the wild-type enzyme, with the resultant k_{cat}/K_M being reduced by ~3-fold. These are relatively small changes, indicating that any intersubunit interactions are not critical for the activity of the enzyme. Further evidence that the monomer provides a good model of the wild-type tetramer was sought through X-ray crystallographic studies.

Structural Characterization of Monomeric CstII. CD spectroscopy and X-ray crystallography were used to characterize CstII-F121D and CstII-Y125Q. The CD spectra of wild-type CstII, CstII-F121D, and CstII-Y125Q revealed that the secondary structures of the mutants were not significantly altered by the mutations (data not shown). However, the midpoint unfolding temperatures (T_m) of both mutants were substantially lower than that of the wild-type protein, indicating a loss of stability, as would be expected for a monomer compared to its native tetrameric form. As summarized in Table 2, CstII-F121D was both slightly more stable and, in practical terms, better behaved (i.e., more soluble and less prone to aggregation during NMR measurements) than CstII-Y125Q. This is likely a result of the additional surface charge introduced by this mutation.

CstII-Y125Q crystallized with one molecule in the asymmetric unit. However, the application of 4-fold crystallographic symmetry reconstitutes a tetramer very similar to that observed for wild-type CstII (0.68 Å rms deviation for 699 Cα atoms). Although monomeric in solution as confirmed by analytical gel filtration chromatography and static light scattering experiments, this suggests that the CstII-Y125Q mutant still has the ability to form a tetramer in the crystal lattice under specific crystallization conditions. In comparison to wild-type CstII, there was no significant change in secondary, tertiary, or crystallographically generated quaternary structure due to the mutation (Figure 4A). Indeed, even the α-helix in which residue 125 is located was not altered in any appreciable way. Interestingly, although the sugar donor analogue CMP-3FNeu5Ac is observed in the active site of CstII-Y125Q, the electron density of part of the lid domain (residues 157−161 and 180−186) was missing. This is indicative of conformational disorder within a portion of the CstII active site.

NMR Spectroscopic Studies of CstII Monomeric Mutants. The $^1H/^{15}N$-HSQC NMR spectra of wild-type CstII, CstII-F121D, and CstII-Y125Q were obtained (Figure 5). Ideally, each of these spectra should contain ~300 peaks arising from the backbone and side-chain amide/indole $^1H-^{15}N$ pairs within the 269-residue protein. However, as expected from its high molecular mass, the spectrum of tetrameric wild-type CstII only showed a small number of broad signals, most of which arise from flexible asparagine and glutamine $^{15}NH_2$ groups

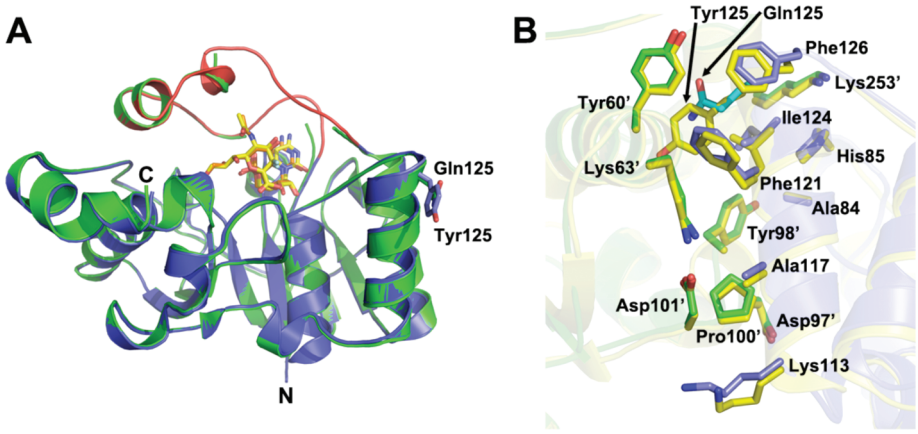

FIGURE 4: (A) Superimposed structures of wild-type CstII (blue, red) and CstII-Y125Q (green) complexed with the sugar donor analogue CMP-3FNeu5Ac. Tyr125 in wild-type CstII and Gln125 in CstII-Y125Q are shown as stick models. Carbon atoms are in yellow and orange for CMP-3FNeu5Ac bound to wild-type CstII and CstII-Y125Q mutant, respectively. The lid domain (residues 155−188) of the wild-type CstII is identified in red. All non-carbon atoms are colored according to type (N, blue; O, red; F, cyan; P, orange). (B) Structural alignment of the interface between two monomer subunits of the wild-type CstII and CstII-Y125Q. The core interfacial residues are shown as stick models. Residues (primed) from adjacent monomers of CstII-Y125Q are colored in blue and green for carbon atoms, respectively. Corresponding residues of wild-type CstII are displayed in yellow for carbon atoms, with the exception of Gln125 in cyan. Non-carbons are identified according to atom type (N, blue; O, red).

Table 2: Screening of CstII Mutants for Oligomerization and Activity

mutation	expression[a]	oligomerization state[b]	activity[c]	T_m[d] (°C)
wild type	yes	tetramer	yes	62
K63D	yes	tetramer	yes	
D97A	yes	tetramer	yes	
F121D	yes	monomer	yes	53
Y125Q	yes	monomer	yes	49
K253Q	yes	monomer/dimer	yes	
F121D/Y125Q	yes	monomer	no	
K63D/F121D	no			
D97A/Y125Q	yes	monomer	no	
Y125Q/K253Q	yes	monomer	no	
K63D/D97A/F121D	no			
K63D/F121D/K253Q	no			
D97A/Y125Q/K253Q	yes	monomer	no	
K63D/F121D/Y125Q	no			
K63D/D97A/F121D/Y125Q	no			
F121D/I124D/Y125D/F126D	yes	monomer	no	
K63D/D97A/F121D/Y125Q/K253Q	no			

[a]Expression measured by SDS−PAGE of whole cell lysates after 16 h of induction at 30 °C. [b]Oligomerization state determined by analytical gel filtration chromatography (22 °C) in pH 7.5 sample buffer. [c]Activity of unpurified cell lysates measured qualitatively by a TLC fluorescence assay. [d]T_m values determined from thermal unfolding curves monitored by CD spectroscopy at λ = 220 nm (20 mM Tris, 150 mM NaCl, 5 mM DTT, pH 7.5). CstII does not refold reversibly under these conditions.

Table 3: Steady-State Kinetic Parameters for Wild-Type CstII and Monomeric CstII-Y125Q[a]

	K_M (μM)	k_{cat} (min^{-1})	k_{cat}/K_M (μM^{-1} min^{-1})
WT CstII	440	60	0.14
CstII-Y125Q	170	8	0.05

[a]Data for sugar donor CMP-Neu5Ac in the presence of 160 mM acceptor lactose at pH 7.5 and 37 °C.

(Figure 5A). In contrast, the spectra of CstII-F121D and CstII-Y125Q each contained ~150 signals (Figure 5B,C). This is consistent with complementary experiments demonstrating that the two mutants are predominantly monomeric. However, the absence of approximately half of the expected signals is suggestive of extensive conformational exchange broadening, either due to millisecond to microsecond time scale motions within the monomers or due to an equilibrium with higher order oligomeric forms. Parenthetically, the peaks in the spectrum of CstII-F121D were generally more intense and sharper than those in the spectrum of CstII-Y125Q, which may correlate with the higher stability and solubility of the former species. Although CstII-F121D was found to behave better, CstII-Y125Q was generated first and thus used for initial NMR analyses. The $^1H/^{15}N$-HSQC NMR spectrum of CstII-Y125Q with saturated CMP-3FNeu5Ac was also recorded in the hope that ligand binding would improve its spectra (not shown). Unfortunately, there was no change in the overall number of signals, and small chemical shift perturbations relative to the apo species were observed for only a limited number of the resonances.

$^1H/^{13}C$-methyl-TROSY spectra of selectively leucine, valine, and isoleucine [$^2H/^{13}C$]methyl-labeled CstII-Y125Q with and without substrates were also obtained (Figure 6). There are 19 isoleucine, 25 leucine, and 7 valine residues in the protein; thus in the most favorable case, 83 peaks should be observable. In the

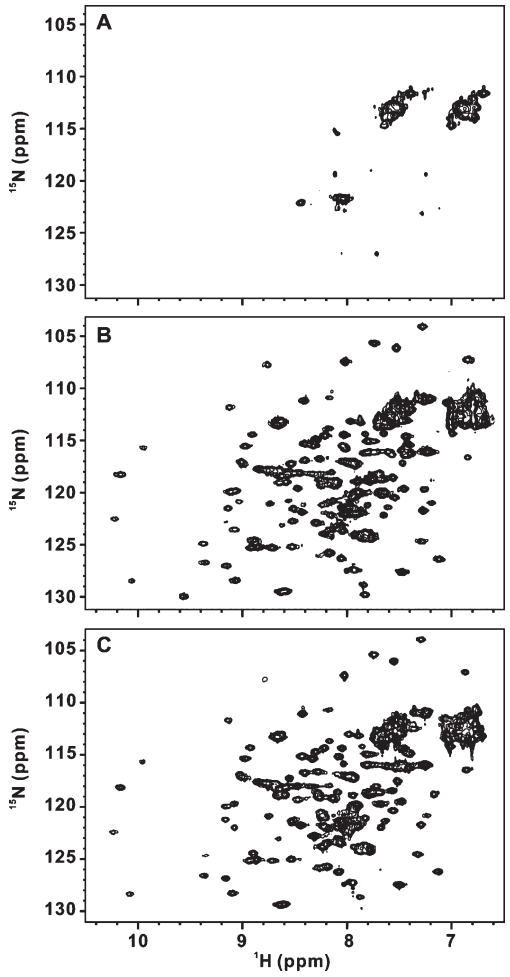

FIGURE 5: ^{1}H/^{15}N-HSQC spectra of ^{15}N-labeled (A) tetrameric His$_6$-tagged CstII, (B) monomeric His$_6$-tagged CstII-F121D, and (C) monomeric CstII-Y125Q in pH 7.5 at 25 °C. Of ~300 expected $^{1}H^{N}-^{15}N$ cross peaks, only ~150 are observed in the spectra of the monomeric species, thus suggestive of extensive conformational exchange broadening. Addition of CMP-3FNeu5Ac only causes minor spectral perturbations (not shown).

spectrum of the apoprotein, only ~70 peaks were observed. Although this may in part be due to chemical shift degeneracy, the absence of ~15% of the expected signals is again indicative of some conformational exchange broadening. In contrast, ~80 peaks are observed when CstII-Y125Q is bound to CMP-3FNeu5Ac, suggesting that inhibitor binding may increase the overall chemical shift dispersion due to conformational perturbations or may dampen motions of the enzyme leading to the postulated exchange broadening. Addition of acceptor substrate lactose did not lead to any further measurable changes (not shown). Unfortunately, the lack of observable $^{1}H-^{15}N$ signals from many backbone amides precluded the assignment of these methyl signals by established main chain directed methods (*33*).

NMR Determination of the pK_a Value of His188. To directly measure the pK_a value of His188, a sample of CstII-F121D selectively labeled with [$^{13}C^{\varepsilon 1}$]histidine was prepared (*42*). This protein was also deuterated, and measurements were carried out in D_2O buffer to minimize possible adverse relaxation from background protons. CstII-F121D contains 6 histidines, yet only 5 signals were detected in its ^{1}H/^{13}C-HSQC spectrum (Figure 7A). Fortunately, one of these was assigned to His188 due to its absence in the corresponding spectrum of CstII-F121D-H188A

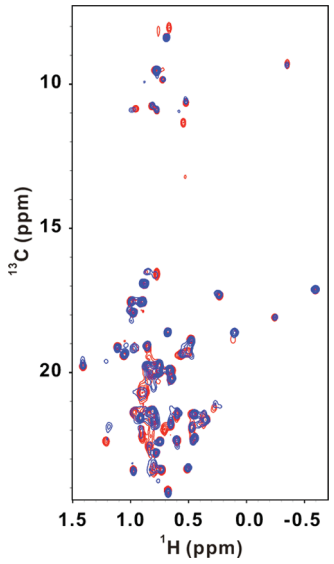

FIGURE 6: Overlaid ^{1}H/^{13}C-methyl-TROSY spectra of uniformly deuterated and ^{1}H/^{13}C selectively methyl labeled CstII-Y125Q in its apo form (red) and in the presence of 5 mM CMP-3FNeu5Ac (blue) in D_2O buffer. Only signals from the methyl groups of leucine ($\delta 1$ and $\delta 2$), valine ($\gamma 1$ and $\gamma 2$), and isoleucine ($\delta 1$; most upfield in ^{13}C) are detected. In CstII-Y125Q, there are 19 isoleucine, 25 leucine, and 7 valine residues, and thus ideally, 83 peaks should be observed in each spectrum. In the apo spectrum, ~70 peaks are observed, whereas ~80 peaks are observed in the spectrum of CMP-3FNeu5Ac-bound CstII. Addition of 160 mM lactose did not cause any further spectral changes (not shown).

(Figure 7A). The remaining signals, labeled as peaks A–D, remain unassigned.

The ^{1}H/^{13}C-HSQC spectra of CstII-F121D and CstII-F121D-H188A were recorded as a function of pH. Over the course of these titrations, the signals from His188, peak A, and peak B could be followed, whereas those from peaks C and D could not be detected at pH* values less than ~7. From the pH dependence of their $^{13}C^{\varepsilon 1}$ and $^{1}H^{\varepsilon 1}$ chemical shifts, the fit pK_a* values were 6.6 ± 0.1 for His188, 6.9 ± 0.1 for peak A, and 6.7 ± 0.1 for peak B (Figure 7B–G). Consistent with its postulated role as a general base, the NMR spectroscopically measured pK_a* value of 6.6 for His188 agrees well with the apparent whole enzyme pK_a of 6.5 determined from the pH dependence of k_{cat}/K_M.

DISCUSSION

The crystal structures of both monofunctional CstI and bifunctional CstII provided important insights into the mode of donor substrate binding, as well as testable hypotheses regarding the inverting mechanism of sialyl transfer. To examine the proposal that His188 serves as the catalytic base, we have used kinetic studies and NMR spectroscopy to investigate the overall dynamic properties of CstII and to determine the pK_a value of this important active site residue.

Monomerization of CstII. Preliminary attempts to measure the pK_a value of His188 in tetrameric wild-type CstII by NMR spectroscopy proved unsuccessful, suggesting that monomerization of the protein would be necessary for this analysis. Fortunately, the active site of CstII is contained entirely within a subunit, thus allowing the generation of active monomers by mutating interfacial hydrophobic residues to polar or charged species (Table 2). Note that the interface between the subunits of CstII contains multiple aromatic residues (i.e., Tyr60, Tyr98, His85, Phe121, Tyr125, and Phe126) indicating that self-association

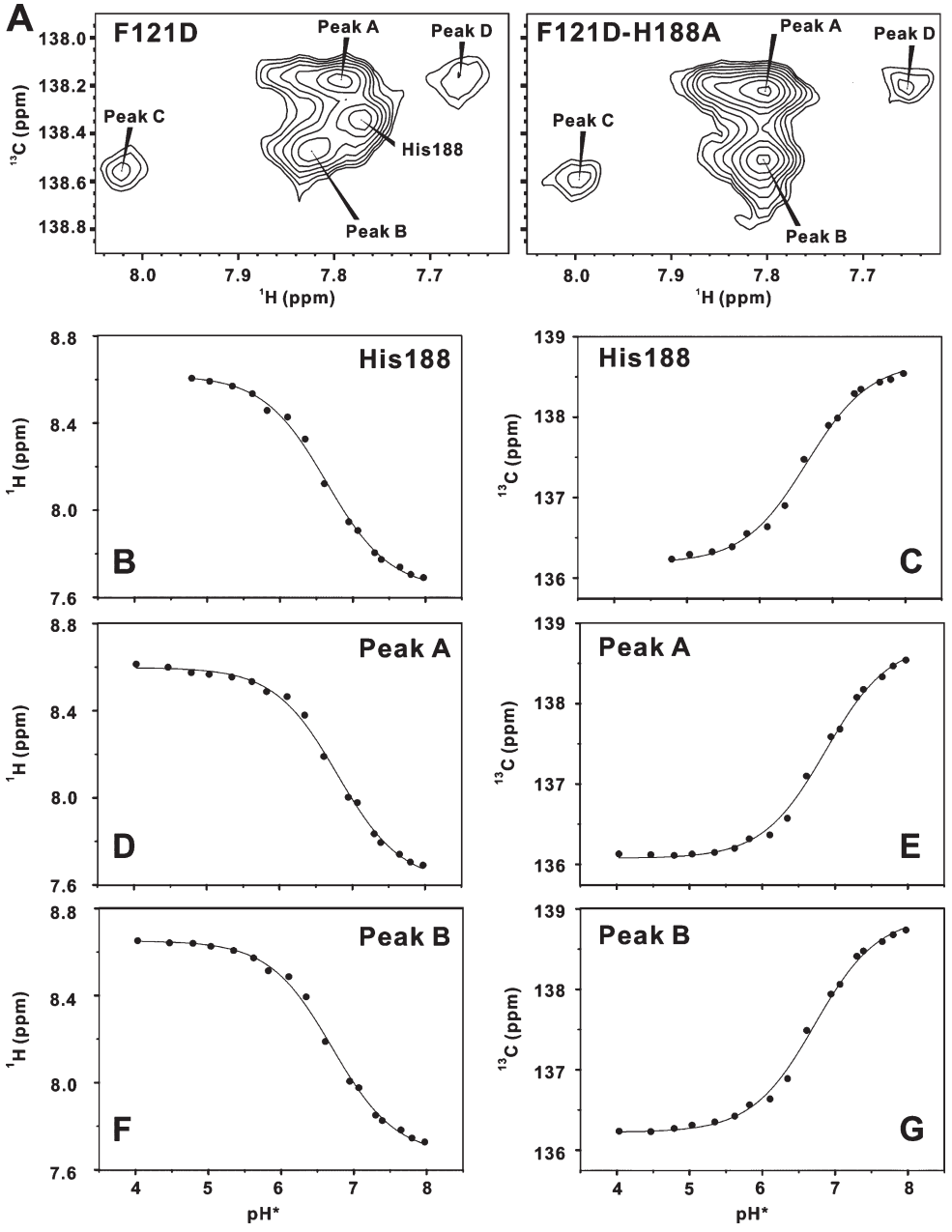

FIGURE 7: Measurement of the pK_a value of His188 by NMR spectroscopy. (A) ^{1}H/^{13}C-HSQC spectra of [$^{13}C^{\varepsilon 1}$]histidine-labeled monomeric CstII-F121D at pH* 7.39 (left) and CstII-F121D-H188A at pH* 7.32 (right) are shown. Five peaks are observed in the spectrum of CstII-F121D, whereas only four peaks are observed with CstII-F121D-H188A. The missing signal corresponds to His188, and the remaining peaks are unassigned. Plots of $^{1}H^{\varepsilon 1}$ chemical shifts against pH* for His188, peak A, and peak B are shown in (B), (D), and (F), respectively. The corresponding plots of $^{13}C^{\varepsilon 1}$ chemical shifts against pH* are shown in (C), (E), and (G), respectively. The lines show fit curves with pK_a* values of 6.6 ± 0.1 for His188, 6.9 ± 0.1 for peak A, and 6.7 ± 0.1 for peak B.

results at least in part from stacking and hydrophobic interactions between these side chains from adjacent monomers. Several of the tested mutants remained tetrameric, while others lost activity upon monomerization. Fortunately, CstII-F121D and CstII-Y125Q were found to be monomeric by gel filtration, static light scattering, and NMR spectroscopic measurements. Both of these variants retained ~30% of the wild-type activity.

The CD spectra of wild-type CstII, CstII-F121D, and CstII-Y125Q were nearly indistinguishable (data not shown), indicating that no significant change in secondary structure results from either mutation. Furthermore, the crystal structure of CstII-Y125Q complexed with CMP-3FNeu5Ac superimposes closely with that of the wild-type protein with no measurable difference in conformation at the crystallographic subunit interface or at the active site. Interestingly, although monomeric in solution, the tetrameric state of CstII-Y125Q is reconstituted by the 4-fold crystallographic axis. This is suggestive of a possible shift in a monomer/tetramer equilibrium toward the tetramer upon crystallization. Even though the sugar donor analogue CMP-3FNeu5Ac was clearly observed in the active site of CstII-Y125Q, electron density from part of the lid domain (residues 157−161 and 180−186) was absent, indicating disorder in this region of the enyzme. In the case of the wild-type protein, the lid domain is also disordered in crystals of its ap*o* form. However, when bound to this analogue, wild-type CstII crystallizes as a tetramer in the asymmetric unit, with the lid domain becoming observable in one of four subunits (*8*, *9*). The differing mobility of the lid domain in these various species may be due to crystal

packing restraints and/or to long-range effects of the mutations (either directly or via self-association equilibria) on the internal dynamics of CstII.

If monomeric CstII-F121D and CstII-Y125Q mutants are active and retain wild-type tertiary structure, why has CstII evolved to exist as a tetramer? This is unlikely to be due to any requirement for allosteric behavior, since no cooperativity has been observed in substrate binding with wild-type enzyme (L. Lairson, Ph.D. Thesis, University of British Columbia, 2007). To analyze for any such effect in the monomerized species, the CstII-Y125Q mutant was assayed with saturating concentrations of donor CMP-Neu5Ac and acceptor lactose as a function of enzyme concentration (0−2.5 μM). A linear relationship was observed between the k_{cat}/K_M and the amount of enzyme (data not shown), also indicating a lack of cooperativity such as that which could result from concentration effects on a monomer/tetramer equilibrium of this mutant species. One possibility is simply that tetramerization confers greater stability. This is consistent with the higher T_m value of wild-type CstII relative to the two monomeric species (Table 2). Alternatively, because its C-terminal membrane association sequences are expected to be aligned along the same face of the tetramer, oligomerization may also be required for effective attachment of CstII to the bacterial inner membrane or interaction with other partner proteins involved in the synthesis or export of LOS (*8*, *9*).

NMR Spectroscopic Analysis of Monomeric Forms of CstII. The $^1H/^{15}N$-HSQC spectra of CstII-F121D and CstII-Y125Q are obviously improved compared with that of the tetrameric wild-type enzyme, confirming that the two mutants are predominantly monomeric and folded properly (Figure 5). Of the two variants, the $^1H/^{15}N$-HSQC spectrum of CstII-F121D is slightly better than that of CstII-Y125Q. This is consistent with the greater stability of CstII-F121D relative to CstII-Y125Q, as measured by T_m values (Table 2) and by the observation that the former species is less prone to aggregation at the concentrations (~100 μM) used for NMR measurements. Given the remoteness of residue 125 from the active site, significant differences in structure and enzymatic mechanism between these two mutants would not be anticipated.

Although monomerization of CstII vastly improved its $^1H/^{15}N$-HSQC spectra, approximately half of the expected $^1H^N-^{15}N$ cross-peaks still remained undetected. The absence of these signals is unlikely to be a simple result of the ~30 kDa mass of CstII-F121D and CstII-Y125Q (albeit rather large for NMR analysis) as the relaxation properties of all residues within well-ordered regions of a globular protein should be comparable. Furthermore, $^1H/^{15}N$-TROSY-HSQC spectra of uniformly deuterated samples of CstII-Y125Q were not significantly improved relative to standard $^1H/^{15}N$-HSQC spectra, indicating that this is not simply a problem of rapid relaxation due to high molecular mass (data not shown).

The absence of numerous $^1H/^{15}N$-HSQC signals likely results from conformational exchange broadening on the chemical shift (millisecond to microsecond) time scale. This could arise from two pathways. The first of these might involve internal backbone motions of regions of monomeric CstII. Of course, it is tempting to speculate that such motions might be important for enzymatic activity. Indeed, in the crystal structure of wild-type CstII, the lid domain lacks detectable electron density in the apoprotein and is observed in only one out of four monomer units when bound with CMP-3FNeu5Ac (*8*, *9*). This indicates that the lid domain is indeed dynamic and that inhibitor binding does alter the structure and mobility of the CstII active site, at least in the crystalline state. However, the lid domain remained disordered in the crystal structure of CstII-Y125Q in complex with CMP-3FNeu5Ac, and the $^1H/^{15}N$-HSQC spectra of both monomeric mutants in the presence of saturating CMP-3FNeu5Ac were of similar quality to those obtained without any bound ligands (not shown). Thus, motions of the lid domain associated with crystallographic disorder may occur on time scales other than those leading to the postulated $^1H/^{15}N$-HSQC exchange broadening. An alternative explanation for the missing NMR signals could be an equilibrium with a sufficient population of tetramers (or other oligomeric forms) to alter the relaxation properties of residues whose chemical shifts differ between these species. Although no evidence for tetramer formation was obtained from analytical gel filtration chromatography and static light scattering experiments, these measurements were carried out at concentrations lower than those used for NMR experiments. Distinguishing these two pathways will require additional studies, including the assignment of the ~150 peaks detectable in the $^1H/^{15}N$-HSQC spectra of CstII-Y125Q or CstII-F121D.

$^1H/^{13}C$-methyl-TROSY spectra of background-deuterated, selectively [$^1H/^{13}C$]methyl-labeled CstII-Y125Q with and without substrates were also obtained (Figure 6). Interestingly, most of the expected methyl signals were detected in the spectra of this monomeric mutant, indicating that the chemical shifts of these side chain moieties are less sensitive than those of the backbone amides to any postulated conformational exchange in CstII. Although unassigned, the ~13 missing peaks in the $^1H/^{13}C$-methyl-TROSY spectrum of the apoenzyme might be associated with the flexible lid domain, as essentially the full complement of expected signals is detected in the presence of saturating amounts of the stable donor substrate analogue CMP-3FNeu5Ac. [^{13}C]Methyl relaxation dispersion experiments, which sensitively detect conformational exchange on the millisecond to microsecond time scale, were also carried out with selectively [$^2H/^{13}C$]methyl-labeled CstII-Y125Q (not shown). Of the ~70 detectable methyl groups in the apoenzyme, ~18 showed dispersion profiles indicative of conformational exchange. However, upon addition of 5 mM CMP-3FNeu5Ac, only 3 of these methyl groups showed reduced dispersion suggestive of dampened motions. Conversely, ~19 out of ~80 methyl groups in the substrate-bound enzyme still exhibited dispersion profiles, and 4 of these did not show any such behavior in the apo form. Together, these NMR spectroscopic and X-ray crystallographic data suggest that CstII exhibits a complex repertoire of dynamics in both its unbound and CMP-3FNeu5Ac-bound states.

Catalytic His188. In glycosidases and inverting glycosyltransferases, with some exceptions, the role of the catalytic general base is typically played by the side chain carboxylate group of a glutamate or aspartate residue (*12*, *43*). However, in the crystal structure of CstII complexed with CMP-3FNeu5Ac, there are no suitably disposed carboxylate groups in the active site. The closest is that of Glu57, which is 14 Å away from the anomeric reaction center. Of the side chains situated adjacent to the anomeric carbon of CMP-3FNeu5Ac (Figure 1B; Asn31 (3.9 Å), Asn51 (4.0 Å), Ser132 (6.0 Å), and His188 (4.8 Å)), His188 is the only feasible general base candidate (*8*). This residue is situated appropriately on the α-face of the donor sugar and adjacent to an open cleft in the enzyme, which would be the most obvious site to bind the acceptor sugar. Thus, the imidazole side chain is suitably positioned to act as the base in catalysis, deprotonating the incoming hydroxyl group of the acceptor

during nucleophilic attack at the anomeric carbon of the donor sugar. Consistent with this key proposed catalytic role, mutation of His188 to alanine results in a loss of all detectable CstII transferase activities (*8*). Further precedence for the role of His188 as the base catalyst derives from the fact that side chain imidazoles are found to play this role in other classes of enzymes (*44*, *45*). In particular, studies on several human ST's (ST3Gal-I, ST8Sia-II, and ST8Sia-IV) have revealed the identity of an invariant histidine residue that is essential for enzymatic activity (*46*, *47*). The recently reported crystal structures of sialyltransferases CstI (*9*) and *Pm*ST1 (*48*) also revealed active site histidine residues with nearly identical positioning to that of His188 in CstII. Whether the histidine residue functions as the base in the case of *Pm*ST1 is unclear.

Another possible candidate for the base catalyst is the carboxylate moiety of the donor substrate itself (Figure 1). This contention is supported by the complete absence of positively charged residues in the immediate vicinity of the carboxylate, in contrast to what is seen with sialidases, which feature three arginines surrounding the substrate carboxylate (*49*−*52*). Thus, the substrate carboxyl would be expected to have an elevated pK_a value when bound to CstII. However, the observed in-plane conformation of the carboxylate is not consistent with a role as base catalyst, as such a role would require that the moiety be oriented perpendicular to the ring plane (Figure 1B). While it is still possible that its conformation could change upon formation of a ternary complex with the acceptor sugar, it is interesting to note that this near-planar conformation of the carboxylate is what has been predicted by *ab initio* calculations and supported by kinetic isotope effect (KIE) experiments to exist during the transition state for the formation of a sialyloxocarbenium ion during the spontaneous hydrolysis of CMP-Neu5Ac (*53*). Additionally, more recent KIE experiments have cast serious doubt on the ability of the carboxylate of CMP-Neu5Ac to function as an intramolecular base catalyst during spontaneous hydrolysis (*54*).

Consistent with a mechanism involving a general base catalyst, k_{cat}/K_M for wild-type CstII increases with rising pH and displays an apparent pK_a value of 6.5 ± 0.1. Note that k_{cat}/K_M is the second- order rate constant for the reaction of free enzyme and substrate, and thus this value could reflect a deprotonation event in either CstII or CMP-Neu5Ac. Since the CMP-Neu5Ac carboxylic acid moiety has a distinctly lower pK_a value of 2.6 (*55*), it is reasonable to assign this kinetically relevant pK_a of 6.5 to the general base in CstII. Such a value could correspond to a histidine with a relatively "normal" pK_a or to an aspartic or glutamic acid with a moderately perturbed pK_a. Based on NMR-monitored pH titrations, His188 has a site-specific pK_a* value of 6.6 ± 0.1. This is in close agreement with the pK_a value governing the pH dependence of k_{cat}/K_M. In parallel with crystallographic studies and the observed chemical rescue of the H188A mutant, these data strongly support the hypothesis that CstII indeed employs His188 as the general base in a direct displacement S_N2-like inverting mechanism.

ACKNOWLEDGMENT

We thank Mark Okon for assisting with NMR spectroscopy, Cecilia Chiu and Lisa Willis for preliminary experiments, and Matthew Caines for performing the static light scattering analysis. We also thank the X-ray Crystallography Hub at the Centre for Blood Research (University of British Columbia).

SUPPORTING INFORMATION AVAILABLE

A supplementary figure showing the static light scattering data. This material is available free of charge via the Internet at http://pubs.acs.org.

REFERENCES

1. Cantarel, B. L., Coutinho, P. M., Rancurel, C., Bernard, T., Lombard, V., and Henrissat, B. (2009) The carbohydrate-active enzymes database (CAZy): an expert resource for glycogenomics. *Nucleic Acids Res. 37*, D233–238.
2. Lloyd, K. O., and Furukawa, K. (1998) Biosynthesis and functions of gangliosides: recent advances. *Glycoconjugate J. 15*, 627–636.
3. Razi, N., and Varki, A. (1998) Masking and unmasking of the sialic acid-binding lectin activity of CD22 (Siglec-2) on B lymphocytes. *Proc. Natl. Acad. Sci. U.S.A. 95*, 7469–7474.
4. Griffiss, J. M., Schneider, H., Mandrell, R. E., Yamasaki, R., Jarvis, G. A., Kim, J. J., Gibson, B. W., Hamadeh, R., and Apicella, M. A. (1988) Lipooligosaccharides: the principal glycolipids of the neisserial outer membrane. *Rev. Infect. Dis. 10* (Suppl. 2), S287–S295.
5. Vyas, A. A., and Schnaar, R. L. (2001) Brain gangliosides: functional ligands for myelin stability and the control of nerve regeneration. *Biochimie 83*, 677–682.
6. Endtz, H. P., Ang, C. W., van Den Braak, N., Duim, B., Rigter, A., Price, L. J., Woodward, D. L., Rodgers, F. G., Johnson, W. M., Wagenaar, J. A., Jacobs, B. C., Verbrugh, H. A., and van Belkum, A. (2000) Molecular characterization of *Campylobacter jejuni* from patients with Guillain-Barre and Miller Fisher syndromes. *J. Clin. Microbiol. 38*, 2297–2301.
7. Godschalk, P. C., Kuijf, M. L., Li, J., St Michael, F., Ang, C. W., Jacobs, B. C., Karwaski, M. F., Brochu, D., Moterassed, A., Endtz, H. P., van Belkum, A., and Gilbert, M. (2007) Structural characterization of *Campylobacter jejuni* lipooligosaccharide outer cores associated with Guillain-Barre and Miller Fisher syndromes. *Infect. Immun. 75*, 1245–1254.
8. Chiu, C. P., Watts, A. G., Lairson, L. L., Gilbert, M., Lim, D., Wakarchuk, W. W., Withers, S. G., and Strynadka, N. C. (2004) Structural analysis of the sialyltransferase CstII from *Campylobacter jejuni* in complex with a substrate analog. *Nat. Struct. Mol. Biol. 11*, 163–170.
9. Chiu, C. P., Lairson, L. L., Gilbert, M., Wakarchuk, W. W., Withers, S. G., and Strynadka, N. C. (2007) Structural analysis of the α-2,3-sialyltransferase Cst-I from *Campylobacter jejuni* in apo and substrate-analogue bound forms. *Biochemistry 46*, 7196–7204.
10. Gilbert, M., Brisson, J. R., Karwaski, M. F., Michniewicz, J., Cunningham, A. M., Wu, Y., Young, N. M., and Wakarchuk, W. W. (2000) Biosynthesis of ganglioside mimics in *Campylobacter jejuni* OH4384. Identification of the glycosyltransferase genes, enzymatic synthesis of model compounds, and characterization of nanomole amounts by 600 MHz ^{1}H and ^{13}C NMR analysis. *J. Biol. Chem. 275*, 3896–3906.
11. Gilbert, M., Karwaski, M. F., Bernatchez, S., Young, N. M., Taboada, E., Michniewicz, J., Cunningham, A. M., and Wakarchuk, W. W. (2002) The genetic bases for the variation in the lipo-oligosaccharide of the mucosal pathogen, *Campylobacter jejuni*. Biosynthesis of sialylated ganglioside mimics in the core oligosaccharide. *J. Biol. Chem. 277*, 327–337.
12. Lairson, L. L., Henrissat, B., Davies, G. J., and Withers, S. G. (2008) Glycosyltransferases: structures, functions, and mechanisms. *Annu. Rev. Biochem. 77*, 521–555.
13. Sprangers, R., and Kay, L. E. (2007) Quantitative dynamics and binding studies of the 20S proteasome by NMR. *Nature 445*, 618–622.
14. Sprangers, R., and Kay, L. E. (2007) Probing supramolecular structure from measurement of methyl ^{1}H-^{13}C residual dipolar couplings. *J. Am. Chem. Soc. 129*, 12668–12669.
15. Tugarinov, V., and Kay, L. E. (2004) An isotope labeling strategy for methyl TROSY spectroscopy. *J. Biomol. NMR 28*, 165–172.
16. Venter, H., Ashcroft, A. E., Keen, J. N., Henderson, P. J., and Herbert, R. B. (2002) Molecular dissection of membrane-transport proteins: mass spectrometry and sequence determination of the galactose-H^+ symport protein, GalP, of *Escherichia coli* and quantitative assay of the incorporation of [ring-2-^{13}C]histidine and $^{15}NH_3$. *Biochem. J. 363*, 243–252.
17. Waugh, D. S. (1996) Genetic tools for selective labeling of proteins with α-^{15}N-amino acids. *J. Biomol. NMR 8*, 184–192.
18. Wilkins, M. R., Gasteiger, E., Bairoch, A., Sanchez, J. C., Williams, K. L., Appel, R. D., and Hochstrasser, D. F. (1999) Protein identification and analysis tools in the ExPASy server. *Methods Mol. Biol. 112*, 531–552.

19. Aharoni, A., Thieme, K., Chiu, C. P., Buchini, S., Lairson, L. L., Chen, H., Strynadka, N. C., Wakarchuk, W. W., and Withers, S. G. (2006) High-throughput screening methodology for the directed evolution of glycosyltransferases. *Nat. Methods 3*, 609–614.
20. Gosselin, S., Alhussaini, M., Streiff, M. B., Takabayashi, K., and Palcic, M. M. (1994) A continuous spectrophotometric assay for glycosyltransferases. *Anal. Biochem. 220*, 92–97.
21. Pace, C. N. (1990) Measuring and increasing protein stability. *Trends Biotechnol. 8*, 93–98.
22. Leslie, A. G. (2006) The integration of macromolecular diffraction data. *Acta Crystallogr., Sect. D: Biol. Crystallogr. 62*, 48–57.
23. (1994) The CCP4 suite: programs for protein crystallography, Acta Crystallogr., Sect. D: Biol. Crystallogr. 50, 760−763.
24. McCoy, A. J. (2007) Solving structures of protein complexes by molecular replacement with Phaser. *Acta Crystallogr., Sect. D: Biol. Crystallogr. 63*, 32–41.
25. Emsley, P., and Cowtan, K. (2004) COOT: model-building tools for molecular graphics. *Acta Crystallogr., Sect. D: Biol. Crystallogr. 60*, 2126–2132.
26. Murshudov, G. N., Vagin, A. A., and Dodson, E. J. (1997) Refinement of macromolecular structures by the maximum-likelihood method. *Acta Crystallogr., Sect. D: Biol. Crystallogr. 53*, 240–255.
27. Davis, I. W., Leaver-Fay, A., Chen, V. B., Block, J. N., Kapral, G. J., Wang, X., Murray, L. W., Arendall, W. B.III, Snoeyink, J., Richardson, J. S., and Richardson, D. C. (2007) MolProbity: all-atom contacts and structure validation for proteins and nucleic acids. *Nucleic Acids Res. 35*, W375–383.
28. Schuttelkopf, A. W., and van Aalten, D. M. (2004) PRODRG: a tool for high-throughput crystallography of protein-ligand complexes. *Acta Crystallogr., Sect. D: Biol. Crystallogr. 60*, 1355–1363.
29. DeLano, W. L., and Lam, J. W. (2005) PyMOL: A communications tool for computational models. *Abstracts Pap. Am. Chem. Soc. 230*, U1371–U1372.
30. Delaglio, F., Grzesiek, S., Vuister, G. W., Zhu, G., Pfeifer, J., and Bax, A. (1995) NMRPipe: a multidimensional spectral processing system based on UNIX pipes. *J. Biomol. NMR 6*, 277–293.
31. Goddard, T. D., and Kneeler, D. G. (1999) Sparky 3, University of California, San Francisco.
32. Kay, L. E., Keifer, P., and Saarinen, T. (1992) Pure absorption gradient enhanced heteronuclear single quantum correlation spectroscopy with improved sensitivity. *J. Am. Chem. Soc. 114*, 10663–10665.
33. Tugarinov, V., and Kay, L. E. (2003) Ile, Leu, and Val methyl assignments of the 723-residue malate synthase G using a new labeling strategy and novel NMR methods. *J. Am. Chem. Soc. 125*, 13868–13878.
34. Sprangers, R., Li, X., Mao, X., Rubinstein, J. L., Schimmer, A. D., and Kay, L. E. (2008) TROSY-based NMR evidence for a novel class of 20S proteasome inhibitors. *Biochemistry 47*, 6727–6734.
35. Mulder, F. A. A., Spronk, C. A. E. M., Slijper, M., Kaptein, R., and Boelens, R. (1996) Improved HSQC experiments for the observation of exchange broadened signals. *J. Biomol. NMR 8*, 223–228.
36. Bundi, A., and Wüthrich, K. (1979) H-1-NMR parameters of the common amino-acid residues measured in aqueous-solutions of the linear tetrapeptides H-Gly-Gly-X-L-Ala-OH. *Biopolymers 18*, 285–297.
37. Macleod, A. M., Lindhorst, T., Withers, S. G., and Warren, R. A. J. (1994) The acid/base catalyst in the exoglucanase/xylanase from *Cellulomonas fimi* is glutamic acid 127—evidence from detailed kinetic studies of mutants. *Biochemistry 33*, 6371–6376.
38. Viladot, J. L., de Ramon, E., Durany, O., and Planas, A. (1994) Probing the mechanism of *Bacillus* 1,3-1,4-beta-D-glucan 4-glucanohydrolases by chemical rescue of inactive mutants at catalytically essential residues. *Biochemistry 37*, 11332–11342.
39. Zechel, D. L., and Withers, S. G. (2000) Glycosidase mechanisms: anatomy of a finely tuned catalyst. *Acc. Chem. Res. 33*, 11–18.
40. Monegal, A., and Planas, A. (2006) Chemical rescue of α-3-galactosyltransferase. Implications in the mechanism of retaining glycosyltransferases. *J. Am. Chem. Soc. 128*, 16030–16031.
41. Reynolds, C., Damerell, D., and Jones, S. (2009) ProtorP: a protein-protein interaction analysis server. *Bioinformatics 25*, 413–414.
42. Schubert, M., Poon, D. K. Y., Wicki, J., Tarling, C. A., Kwan, E. M., Nielsen, J. E., Withers, S. G., and McIntosh, L. P. (2007) Probing electrostatic interactions along the reaction pathway of a glycoside hydrolase: histidine characterization by NMR spectroscopy. *Biochemistry 46*, 7383–7395.
43. Zechel, D. L., and Withers, S. G. (2001) Dissection of nucleophilic and acid-base catalysis in glycosidases. *Curr. Opin. Chem. Biol. 5*, 643–649.
44. Whiteson, K. L., Chen, Y., Chopra, N., Raymond, A. C., and Rice, P. A. (2007) Identification of a potential general acid/base in the reversible phosphoryl transfer reactions catalyzed by tyrosine recombinases: Flp H305. *Chem. Biol. 14*, 121–129.
45. Legler, P. M., Massiah, M. A., and Mildvan, A. S. (2002) Mutational, kinetic, and NMR studies of the mechanism of *E. coli* GDP-mannose mannosyl hydrolase, an unusual Nudix enzyme. *Biochemistry 41*, 10834–10848.
46. Jeanneau, C., Chazalet, V., Auge, C., Soumpasis, D. M., Harduin-Lepers, A., Delannoy, P., Imberty, A., and Breton, C. (2004) Structure-function analysis of the human sialyltransferase ST3Gal I: role of N-glycosylation and a novel conserved sialylmotif. *J. Biol. Chem. 279*, 13461–13468.
47. Close, B. E., Mendiratta, S. S., Geiger, K. M., Broom, L. J., Ho, L. L., and Colley, K. J. (2003) The minimal structural domains required for neural cell adhesion molecule polysialylation by PST/ST8Sia IV and STX/ST8Sia II. *J. Biol. Chem. 278*, 30796–30805.
48. Ni, L., Chokhawala, H. A., Cao, H., Henning, R., Ng, L., Huang, S., Yu, H., Chen, X., and Fisher, A. J. (2007) Crystal structures of *Pasteurella multocida* sialyltransferase complexes with acceptor and donor analogues reveal substrate binding sites and catalytic mechanism. *Biochemistry 46*, 6288–6298.
49. Burmeister, W. P., Ruigrok, R. W., and Cusack, S. (1992) The 2.2 Å resolution crystal structure of influenza B neuraminidase and its complex with sialic acid. *EMBO J. 11*, 49–56.
50. Crennell, S., Takimoto, T., Portner, A., and Taylor, G. (2000) Crystal structure of the multifunctional paramyxovirus hemagglutinin-neuraminidase. *Nat. Struct. Biol. 7*, 1068–1074.
51. Luo, Y., Li, S. C., Chou, M. Y., Li, Y. T., and Luo, M. (1998) The crystal structure of an intramolecular trans-sialidase with a NeuAc alpha2→3Gal specificity. *Structure 6*, 521–530.
52. Amaya, M. F., Buschiazzo, A., Nguyen, T., and Alzari, P. M. (2003) The high resolution structures of free and inhibitor-bound *Trypanosoma rangeli* sialidase and its comparison with *T. cruzi* trans-sialidase. *J. Mol. Biol. 325*, 773–784.
53. Horenstein, B. A. (1997) Quantum mechanical analysis of an alpha-carboxylate-substituted oxocarbenium ion. Isotope effects for formation of the sialyl cation and the origin of an unusually large secondary C-14 isotope effect. *J. Am. Chem. Soc. 119*, 1101–1107.
54. Horenstein, B. A., and Bruner, M. (1998) The N-acetyl neuraminyl oxocarbenium ion is an intermediate in the presence of anionic nucleophiles. *J. Am. Chem. Soc. 120*, 1357–1362.
55. Vimr, E. R., Kalivoda, K. A., Deszo, E. L., and Steenbergen, S. M. (2004) Diversity of microbial sialic acid metabolism. *Microbiol. Mol. Biol. Rev. 68*, 132–153.